Journal of Photochemistry and Photobiology A: Chemistry 222 (2011) 336–342

Contents lists available at ScienceDirect

Journal of Photochemistry and Photobiology A: Chemistry

journal homepage: www.elsevier.com/locate/jphotochem

Photoluminescence properties of fluorone dyes in bio-related films at low temperatures

Taiju Tsuboi[a], A. Penzkofer[b,*], E. Slyusareva[c], A. Sizykh[c]

[a] Faculty of Engineering, Kyoto Sangyo University, Kamigamo, Kita-ku, Kyoto 603-8555, Japan
[b] Fakultät für Physik, Universität Regensburg, Universitätsstrasse 31, D-93053 Regensburg, Germany
[c] Siberian Federal University, Pr. Svobodnyi. 79, 660041 Krasnoyarsk, Russia

ARTICLE INFO

Article history:
Received 13 April 2011
Received in revised form 7 July 2011
Accepted 9 July 2011
Available online 20 July 2011

Keywords:
Disodium fluorescein
4,5-Dibromofluorescein
Eosin Y
Erythrosine B
Rose bengal
Low-temperature fluorescence
Low-temperature phosphorescence
Internal conversion
Intersystem-crossing

ABSTRACT

The fluorescence and phosphorescence behavior of the fluorone dyes disodium fluorescein (uranine), 4,5-dibromofluorescein, eosin Y, erythrosine B, and rose bengal in biofilms of chitosan, gelatin, and starch was studied in the temperature range from 293 K to 12 K. Luminescence quantum yields, fluorescence quantum yields, and triplet quantum yields were determined. The fluorescence quantum yield generally increased with lowering the temperature at a high level of absolute quantum yield, while the phosphorescence quantum yield increased with decreasing temperature at a low level of absolute quantum yield. The strongest phosphorescence was found for erythrosine B in starch where the phosphorescence quantum yield increased from 6% at 293 K to 25% at 12 K. The temperature dependent luminescence behavior is discussed considering radiative and non-radiative transitions in a spectroscopic-state potential energy surface scheme.

1. Introduction

Fluorone dyes are hydroxy-xanthene dyes (they are homologues of fluorescein). From this group the low-temperature luminescence (fluorescence and phosphorescence) of disodium fluorescein (uranine, FL), 4,5-dibromofluorescein (DBF), disodium-2,4,5,7-tetrabromofluorescein (eosin Y, EO), disodium-2,4,5,7-tetraiodofluorescein (erythrosine B, ER), and disodium-3′,4′,5′,6′-tetrachloro-2,4,5,7-tetraiodofluorescein (rose bengal, RB) in biofilms of gelatin (a protein), starch (a polysaccharide) and chitosan (a polyaminosaccharide) is studied here. An absorption and fluorescence spectroscopic characterization of these fluorone dye doped bio-films at room temperature was carried out in [1]. The phosphorescence and delayed fluorescence properties of these samples at room temperature were studied in [2]. The structural formulae of the studied fluorone dyes and biopolymers are displayed in [1].

The application of fluorone dyes as laser dyes, as media for optical recording of information, in labeling and sensing of biomolecules, and in molecular photonics was discussed in [1] and references therein. The fluorone dyes were hosted in aqueous and organic solvents at room temperature and cryogenic temperature, in inorganic sol–gel glasses, organic polymers and biological polymers (see introductory part of [1] for fluorescence spectroscopic applications and introductory part of [2] for phosphorescence spectroscopic characterizations). The use of bio-related films opens a wide range of applications in biology, cosmetology, and pharmaceutics because of their doping possibility with dyes, ease of fabrication, bio-compatibility, and non-toxicity [3,4]. Chitosan scaffolds appear to be suitable for tissue engineering [5–7]. Gelatin and starch are used for immobilization of bioluminescence assays [8].

Fluorescence quantum yields, ϕ_F, of the investigated fluorone dyes FL [9–15], DBF [15,16], EO [12–14,17], ER [12–14,18,19], and RB [13–15,18,19] in some liquid solvents and solid hosts at room temperature and cryogenic temperature are found in the references given. They decrease in the order $\phi_F(FL) > \phi_F(DBF) \geq \phi_F(EO) > \phi_F(ER) \geq \phi_F(RB)$. Reported phosphorescence parameters of the investigated fluorone dyes in various liquid and solid inorganic, organic and biological solvents are collected in Table 1 of [2]. The quantum yield of S_1–T_1 intersystem-crossing increased in the order $\phi_{ISC}(FL) < \phi_{ISC}(DBF) < \phi_{ISC}(EO) < \phi_{ISC}(ER) < \phi_{ISC}(RB)$. The heavy-atom substitution of H atoms of fluorescein increases the singlet–triplet absorption, shortens the T_1–S_0 radiative lifetime, and enhances the singlet–triplet intersystem crossing rate by enhanced spin–orbit coupling [20,21]. The heavy substituent atoms

* Corresponding author. Tel.: +49 941 943 2107; fax: +49 941 943 2754.
E-mail address: alfons.penzkofer@physik.uni-regensburg.de (A. Penzkofer).

1010-6030/$ – see front matter © 2011 Elsevier B.V. All rights reserved.
doi:10.1016/j.jphotochem.2011.07.006

perturb the π–electron state of the dye molecules, resulting in a mixing of the triplet and singlet states. The strength of the coupling is governed by the atomic spin–orbit coupling factor ζ_k of the substituent atom k. ζ_k increases strongly with the atomic number of atom k [20–22] ($\zeta_{Cl} = 595\,cm^{-1}$, $\zeta_{Br} = 2450\,cm^{-1}$, $\zeta_I = 5250\,cm^{-1}$ from [22]). The rate of intersystem crossing is proportional to ζ_k^2 [20–24]. The phosphorescence efficiency generally increased with lowering the temperature, with changing from liquid solution to solid solution, and with de-aerating the samples (avoiding molecular oxygen quenching especially in the case of liquid solutions and porous sol–gel glasses).

Concerning the temperature dependence of the fluorescence quantum yield, the intersystem-crossing efficiency, and the phosphorescence quantum yield of fluorone dyes no conclusive study has been reported. A detailed comparison of the fluorescence and phosphorescence behavior of the selected fluorone dyes in biopolymers at low temperature with the fluorescence and phosphorescence behavior at room temperature is the purpose of the present paper. The obtained results are discussed in a spectroscopic-state potential energy curve model which generally applies to dyes with non-crossing and non-touching S_0 and S_1 potential energy surfaces like laser dyes.

2. Materials and methods

The same samples were used as in [1,2]. The preparation is described in [1]. The fluorone dye doped films were approximately 10 μm thick. The dye concentration in the films was adjusted to approximately 10^{-3} mol dm^{-3}.

Photoluminescence spectra were measured at various temperatures between 12 K and 293 K with a Spex-Fluorolog-3 fluorophotometer. The accuracy of temperature setting was ±1 K. The excitation source was a 450 W cw Xe lamp. The luminescence detection occurred with a R928P photomultiplier tube (high sensitivity in wavelength range from 240 to 850 nm). Corrections were made for the wavelength dependence of the emission spectrometer and the detection photomultiplier. Absolute luminescence quantum distributions were obtained by calibrating the photoluminescence spectra to the absolute fluorescence and phosphorescence quantum distributions at room temperature (20 ± 1 °C) determined in [2].

The Spex-Fluorolog-3 fluorophotometer uses a cw light source for photo-excitation. Therefore the emission detector registers the accumulated luminescence consisting of fluorescence (prompt fluorescence and delayed fluorescence) and phosphorescence. The luminescence quantum distribution, $E_L(\lambda)$, is given by

$$E_L(\lambda) = E_F(\lambda) + E_P(\lambda) = E_{F,prompt}(\lambda) + E_{DF}(\lambda) + E_P(\lambda), \quad (1)$$

where $E_F(\lambda)$, $E_{F,prompt}(\lambda)$, and $E_{DF}(\lambda)$ are the total, the prompt, and the delayed fluorescence quantum distribution, respectively, and $E_P(\lambda)$ is the phosphorescence quantum distribution.

The luminescence quantum yield, ϕ_L, is given by

$$\phi_L = \int_{em} E_L(\lambda)\, d\lambda = \phi_F + \phi_P = \phi_{F,prompt} + \phi_{DF} + \phi_P, \quad (2)$$

where ϕ_F, $\phi_{F,prompt}$, and ϕ_{DF} are the total, the prompt, and the delayed fluorescence quantum yield, respectively, and ϕ_P is the phosphorescence quantum yield. *em* indicates the wavelength range of emission. The phosphorescence emission maximum occurs at longer wavelength than the fluorescence emission maximum. In the long-wavelength region the fluorescence contribution and the phosphorescence contribution overlap. The spectra may be approximately separated by assuming a linear extension of the slope in the logarithmic presentation of the fluorescence spectra in the long-wavelength region [25]. With this approximation the long-wavelength fluorescence tail is given by $E_F(\lambda) = E_F(\lambda_0)\exp[-(\lambda - \lambda_0)/\delta\lambda]$ where λ_0 is positioned at the short-wavelength onset of phosphorescence and $\delta\lambda$ is the slope width of the fluorescence tail. The used Spex-Fluorolog-3 apparatus allows only the determination of the total fluorescence; it cannot separate the prompt and the delayed fluorescence. In the room temperature studies of [2] a Cary Eclipse fluorimeter was used. There the prompt fluorescence was measured by pulsed photo-excitation and immediate emission detection, while the delayed fluorescence and phosphorescence were separately measured by pulsed photo-excitation and delayed emission detection. The observed weak delayed fluorescence was due to thermal activated T_1–S_1 back intersystem-crossing [17,23,26–31] (E-type delayed fluorescence [32,33]). It becomes negligible at low temperatures.

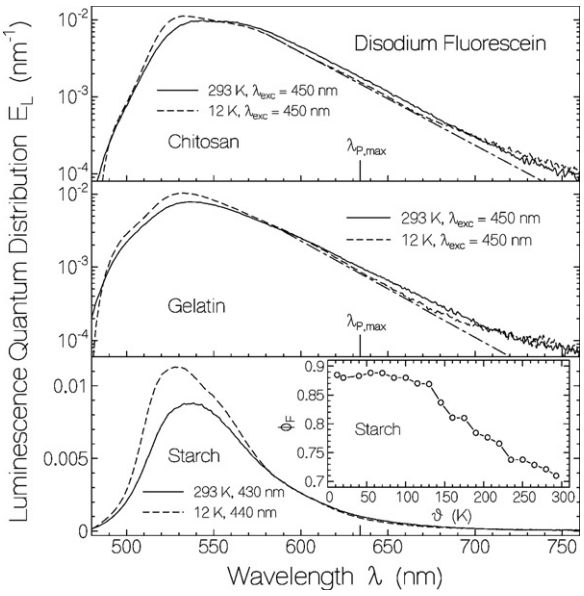

Fig. 1. Luminescence quantum distributions of disodium fluorescein (FL) in chitosan, gelatin, and starch. The applied temperatures and luminescence excitation wavelengths, λ_{exc}, are listed in the legends. $\lambda_{P,max}$ indicates wavelength position of expected maximum phosphorescence emission (taken from [34]). The dash-dotted lines indicate the long-wavelength extension of the fluorescence spectra at 12 K. The inset in the lower part shows the fluorescence quantum yield, ϕ_F, of FL in starch versus temperature.

3. Results

The luminescence quantum distributions, $E_L(\lambda)$, of the investigated fluorone dyes in chitosan, gelatin, and starch at 293 K and at 12 K are displayed in Figs. 1–5. The corresponding luminescence quantum yields and separated fluorescence and phosphorescence quantum yields are listed in Table 1.

The luminescence quantum distribution results for FL are shown in Fig. 1. For all three biopolymer hosts the luminescence quantum yields were high, and cooling of the samples increased the fluorescence efficiency somewhat. The expected wavelength position of maximum phosphorescence, $\lambda_{P,max}$, is indicated in the figures. The value is taken from [34]. At room temperature an upper limit of $\phi_P < 1 \times 10^{-4}$ was determined in [2]. At $\vartheta = 12$ K there is some long-wavelength luminescence tail above the expected fluorescence tail (dash-dotted curves) which may indicate a weak phosphorescence contribution. But the contribution is at the limits of the experimental resolution allowing only the determination of an upper limit of $\phi_P \leq 0.01$. The inset in the lower part of Fig. 1 shows the temperature dependence, $\phi_F(\vartheta)$, of the fluorescence quantum yield of FL in starch over the range from 12 K to 293 K. $\phi_F(\vartheta)$ increased

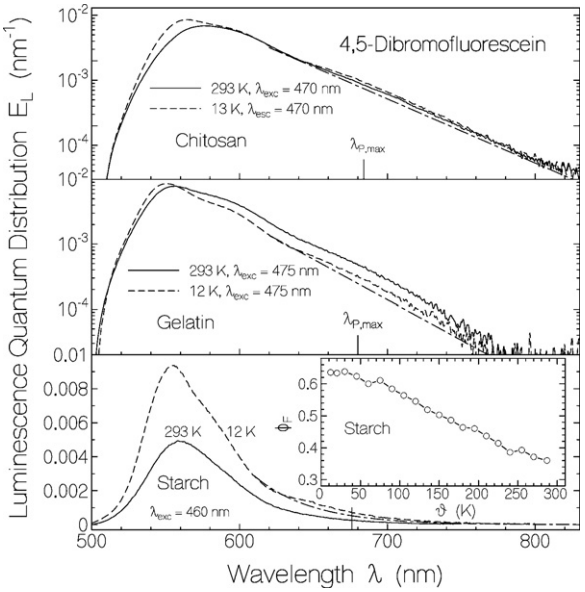

Fig. 2. Luminescence quantum distributions of 4,5-dibromofluorescein (DBF) in chitosan, gelatin, and starch. The applied temperatures and luminescence excitation wavelengths, λ_{exc}, are listed in the legends. $\lambda_{P,max}$ indicates wavelength position of maximum phosphorescence emission (taken from [2]). Dash-dotted curves indicate the long-wavelength fluorescence extension at 12 K. The inset in the lower part shows the fluorescence quantum yield, ϕ_F, of DBF in starch versus temperature.

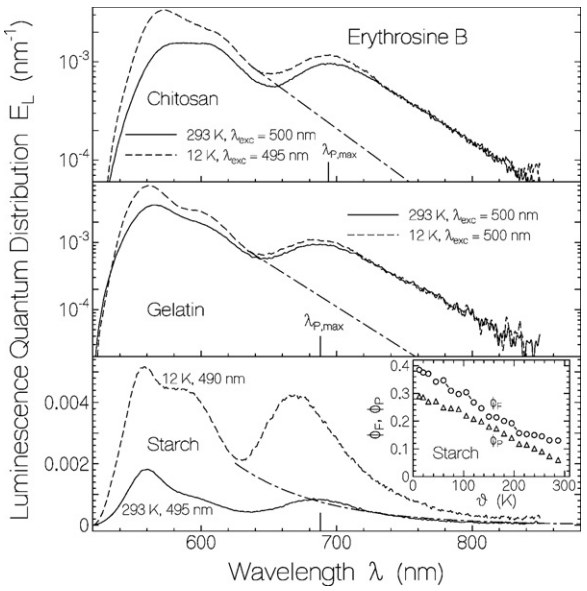

Fig. 4. Luminescence quantum distributions of erythrosine B (ER) in chitosan, gelatin, and starch. The used temperatures and luminescence excitation wavelengths, λ_{exc}, are listed in the legends. $\lambda_{P,max}$ indicates wavelength position of maximum phosphorescence emission (taken from [2]). Dash-dotted curves give the long-wavelength fluorescence extension at 12 K. The inset in the lower part shows the fluorescence quantum yield, ϕ_F, and the phosphorescence quantum yield, ϕ_P, of ER in starch versus temperature.

with decreasing temperature in the region $293\,K > \vartheta > 100\,K$, and remained approximately constant at lower temperature.

The luminescence behavior of DBF in chitosan, gelatin, and starch is shown in Fig. 2. In chitosan the fluorescence quantum yield increased from $\phi_F(293\,K) \approx 0.58$ to $\phi_F(13\,K) \approx 0.66$. In gelatin the fluorescence efficiency decreased from $\phi_F(293\,K) \approx 0.56$ to $\phi_F(12\,K) \approx 0.49$. In starch a strong increase of the fluorescence efficiency from $\phi_F(293\,K) \approx 0.36$ to $\phi_F(12\,K) \approx 0.66$ was observed. At room temperature phosphorescence quantum yields of ϕ_P(gelatin) = 0.0034, ϕ_P(starch) = 0.0022, and ϕ_P(chitosan) = 0.003 were determined in [2]. At 12 K the phosphorescence efficiency increased to $\phi_P \approx 0.0055$ in gelatin (factor of increase $\kappa_{incr} \approx 1.6$), to $\phi_P \approx 0.017$ in starch ($\kappa_{incr} \approx 7.7$), and to $\phi_P \approx 0.016$ in chitosan ($\kappa_{incr} \approx 5.3$). The inset in the lower part of Fig. 2 shows the temperature dependence of the fluorescence quantum yield of DBF in starch in the range from 287 K to 12 K. $\phi_F(\vartheta)$ increased with decreasing temperature in the region $287\,K > \vartheta > 50\,K$, and remained approximately constant at lower temperatures.

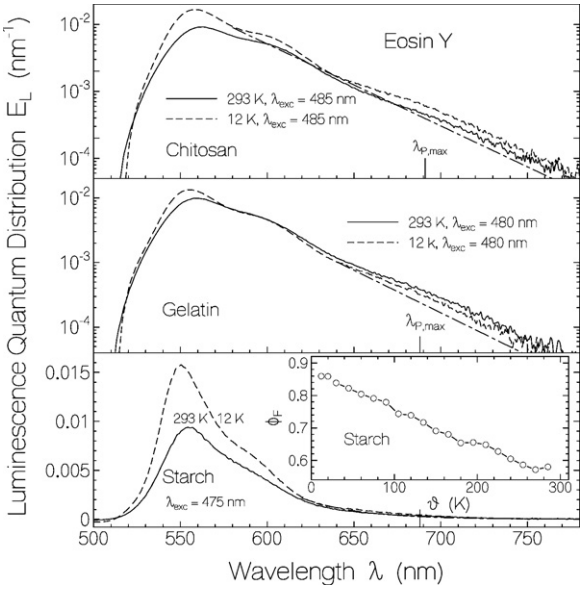

Fig. 3. Luminescence quantum distributions of eosin Y (EO) in chitosan, gelatin, and starch. The used temperatures and luminescence excitation wavelengths, λ_{exc}, are listed in the legends. $\lambda_{P,max}$ indicates wavelength position of maximum phosphorescence emission (taken from [2]). Dash-dotted curves show the long-wavelength fluorescence extension at 12 K. The inset in the lower part shows the fluorescence quantum yield, ϕ_F, of EO in starch versus temperature.

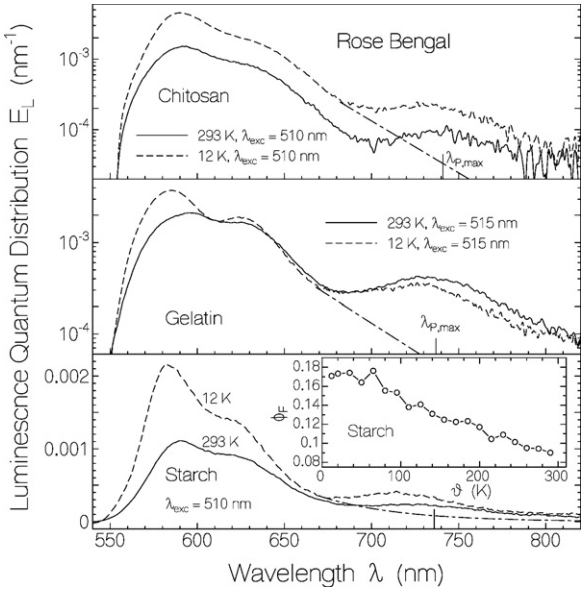

Fig. 5. Luminescence quantum distributions of rose bengal (RB) in chitosan, gelatin, and starch. The used temperatures and luminescence excitation wavelengths, λ_{exc}, are listed in the legends. $\lambda_{P,max}$ indicates wavelength position of maximum phosphorescence emission (taken from [2]). Dash-dotted curves indicate the long-wavelength fluorescence extension at 12 K. The inset in the lower part shows the fluorescence quantum yield, ϕ_F, of RB in starch versus temperature.

Table 1
Photoluminescence parameters of fluorone dyes in bio-related films.

Parameter	Gelatin		Starch		Chitosan	
	293 K	12 K	293 K	12 K	293 K	12 K
Disodium fluorescein						
ϕ_L	0.64 ± 0.03	0.74 ± 0.03	0.71 ± 0.03	0.84 ± 0.03	0.85 ± 0.03	0.87 ± 0.03
ϕ_F	0.64 ± 0.03	0.74 ± 0.03	0.71 ± 0.03	0.84 ± 0.03	0.85 ± 0.03	0.87 ± 0.03
ϕ_P	$<1 \times 10^{-4}$	≤0.01	$<1 \times 10^{-4}$	≤0.01	$<1 \times 10^{-4}$	≤0.007
$\phi_{S_1,nr}$	0.36	0.26	0.29	0.16	0.15	0.13
4,5-Dibromofluorescein						
ϕ_L	0.56 ± 0.03	0.50 ± 0.04	0.36 ± 0.02	0.68 ± 0.03	0.58 ± 0.03	0.68 ± 0.03
ϕ_F	0.56 ± 0.03	0.49 ± 0.04	0.36 ± 0.02	0.66 ± 0.03	0.58 ± 0.03	0.66 ± 0.03
ϕ_P	≈0.0034	≈ 0.0055	≈0.0022	≈0.017	≈0.003	≈0.016
ϕ_{IC,S_1-S_0}	0.292		0.39	>0.09, <0.323	0.244	>0.164, <0.244
ϕ_{ISC,S_1-T_1}	0.148		0.25	>0.017, <0.25	0.176	>0.096, <0.176
$\phi_{S_1,nr}$	0.44	0.51	0.64	0.34	0.42	0.34
ϕ'_P	0.023		0.0088	<1, >0.068	0.017	<0.167, >0.091
ϕ_{ISC,T_1-S_0}	0.977		0.991	>0, <0.932	0.983	>0.833, <0.909
Eosin Y						
ϕ_L	0.62 ± 0.03	0.70 ± 0.03	0.60 ± 0.03	0.88 ± 0.03	0.62 ± 0.03	0.93 ± 0.03
ϕ_F	0.61 ± 0.03	0.69 ± 0.03	0.59 ± 0.03	0.87 ± 0.03	0.61 ± 0.03	0.91 ± 0.03
ϕ_P	0.00635	≈0.0073	0.0055	≈0.013	0.0052	≈0.018
ϕ_{IC,S_1-S_0}	0.207	>0.127, <0.207	0.181	>0, <0.117	0.217	>0, <0.072
ϕ_{ISC,S_1-T_1}	0.183	>0.103, <0.183	0.224	>0.013, <0.13	0.168	>0.018, <0.09
$\phi_{S_1,nr}$	0.39	0.31	0.41	0.13	0.39	0.09
ϕ'_P	0.035	<0.071, >0.04	0.025	<1, >0.1	0.031	<1, >0.2
ϕ_{ISC,T_1-S_0}	0.965	>0.929, <0.96	0.975	>0, <0.9	0.969	>0, <0.8
Erythrosine B						
ϕ_L	0.29 ± 0.03	0.43 ± 0.03	0.18 ± 0.02	0.74 ± 0.03	0.21 ± 0.02	0.32 ± 0.03
ϕ_F	0.22 ± 0.02	0.36 ± 0.03	0.12 ± 0.02	0.49 ± 0.03	0.16 ± 0.02	0.24 ± 0.03
ϕ_P	0.0455	0.071 ± 0.01	0.06	0.25 ± 0.02	0.049	0.076 ± 0.01
ϕ_{IC,S_1-S_0}	0.393	>0.273, <0.393	0.333	>0, <0.26	0.379	>0.299, <0.379
ϕ_{ISC,S_1-T_1}	0.367	>0.247, <0.367	0.557	>0.25, <0.333	0.461	>0.381, <0.461
$\phi_{S_1,nr}$	0.78	0.64	0.88	0.51	0.84	0.76
ϕ'_P	0.124	<0.287, >0.191	0.108	<1, >0.75	0.106	<0.2, >0.165
ϕ_{ISC,T_1-S_0}	0.876	>0.713, <0.809	0.892	>0, <0.25	0.894	>0.8, <0.835
Rose bengal						
ϕ_L	0.19 ± 0.02	0.24 ± 0.02	0.11 ± 0.02	0.18 ± 0.02	0.10 ± 0.02	0.26 ± 0.02
ϕ_F	0.16 ± 0.02	0.21 ± 0.02	0.082 ± 0.02	0.16 ± 0.02	0.089 ± 0.02	0.24 ± 0.02
ϕ_P	0.028	0.025 ± 0.005	0.027	0.022 ± 0.005	0.011	0.014 ± 0.004
ϕ_{IC,S_1-S_0}	0.033	>0, <0.033	0.132	>0.054, <0.132	0.227	>0.076, <0.227
ϕ_{ISC,S_1-T_1}	0.807	>0.757, <0.79	0.786	>0.708, <0.786	0.684	>0.533, <0.684
$\phi_{S_1,nr}$	0.84	0.79	0.918	0.84	0.911	0.76
ϕ'_P	0.035	<0.033, >0.032	0.034	<0.031, >0.028	0.016	<0.026, >0.02
ϕ_{ISC,T_1-S_0}	0.965	>0.967, <0.968	0.966	>0.969, <0.972	0.984	>0.974, <0.98

293 K data are taken from [2]. 12 K data are this work.

The luminescence behavior of EO in chitosan, gelatin, and starch at 293 K and 12 K is depicted in Fig. 3. In all three biopolymers the fluorescence efficiency increased with decreasing temperature (ϕ_F values listed in Table 1). At room temperature phosphorescence quantum yields of ϕ_P(gelatin) = 0.00635, ϕ_P(starch) = 0.0055, and ϕ_P(chitosan) = 0.0052 were determined in [2]. At 12 K the phosphorescence efficiency increased to $\phi_P \approx 0.0073$ in gelatine ($\kappa_{incr} \approx 1.15$), to $\phi_P \approx 0.013$ in starch ($\kappa_{incr} \approx 2.4$), and to $\phi_P \approx 0.018$ in chitosan ($\kappa_{incr} \approx 3.5$). The inset in the lower part of Fig. 3 shows the temperature dependence of the fluorescence quantum yield of EO in starch in the range from 285 K to 12 K. $\phi_F(\vartheta)$ increased monotonically with decreasing temperature over the whole displayed temperature range.

The luminescence behavior of ER in chitosan, gelatin, and starch is depicted in Fig. 4. In all three biopolymers the fluorescence efficiency increased with decreasing temperature ($\phi_F(293\,K) \approx 0.16$ and $\phi_F(12\,K) \approx 0.24$ in chitosan; $\phi_F(293\,K) \approx 0.22$ and $\phi_F(12\,K) \approx 0.36$ in gelatin; $\phi_F(293\,K) \approx 0.12$ and $\phi_F(12\,K) \approx 0.49$ in starch). The phosphorescence emission in the biopolymers is well resolved. In chitosan ($\phi_P(293\,K) \approx 0.049$, $\phi_P(12\,K) \approx 0.076$) and in gelatin ($\phi_P(293\,K) \approx 0.046$, $\phi_P(12\,K) \approx 0.071$) the phosphorescence efficiency increased a factor of $\kappa_{incr} \approx 1.55$ with decreasing temperature. In starch the phosphorescence efficiency increased a factor of $\kappa_{incr} \approx 4.2$ from $\phi_P(293\,K) \approx 0.06$ to $\phi_P(12\,K) \approx 0.25$. The inset in the lower part of Fig. 4 shows the temperature dependence of the fluorescence quantum yield, $\phi_F(\vartheta)$, and of the phosphorescence quantum yield, $\phi_P(\vartheta)$, in starch in the range from 287 K to 12 K. Both, $\phi_F(\vartheta)$ and $\phi_P(\vartheta)$, increased with decreasing temperature over the whole displayed temperature range.

The luminescence behavior of RB in chitosan, gelatin, and starch is depicted in Fig. 5. In all three biopolymers the fluorescence efficiency increased with decreasing temperature ($\phi_F(293\,K) \approx 0.089$ and $\phi_F(12\,K) \approx 0.24$ in chitosan; $\phi_F(293\,K) \approx 0.16$ and $\phi_F(12\,K) \approx 0.21$ in gelatin; $\phi_F(293\,K) \approx 0.082$ and $\phi_F(12\,K) \approx 0.16$ in starch). The phosphorescence emission in the biopolymers is well resolved. In chitosan ($\phi_P(293\,K) \approx 0.011$, $\phi_P(12\,K) \approx 0.014$, $\kappa_{incr} \approx 1.27$), gelatin ($\phi_P(293\,K) \approx 0.028$, $\phi_P(12\,K) \approx 0.025$, $\kappa_{incr} \approx 0.89$), and starch ($\phi_P(293\,K) \approx 0.027$, $\phi_P(12\,K) \approx 0.022$, $\kappa_{incr} \approx 0.81$) the phosphorescence efficiency is nearly unchanged at 293 K and at 12 K. The inset in the lower part of Fig. 5 shows the temperature dependence of the fluorescence quantum yield, $\phi_F(\vartheta)$, in starch in the range from 290 K to 12 K. $\phi_F(\vartheta)$ increased with decreasing temperature in the range from 290 K to 70 K, and remained approximately constant at lower temperatures.

4. Discussion

The experimental results on the photoluminescence of the investigated fluorone dyes in solid biopolymer films as a function

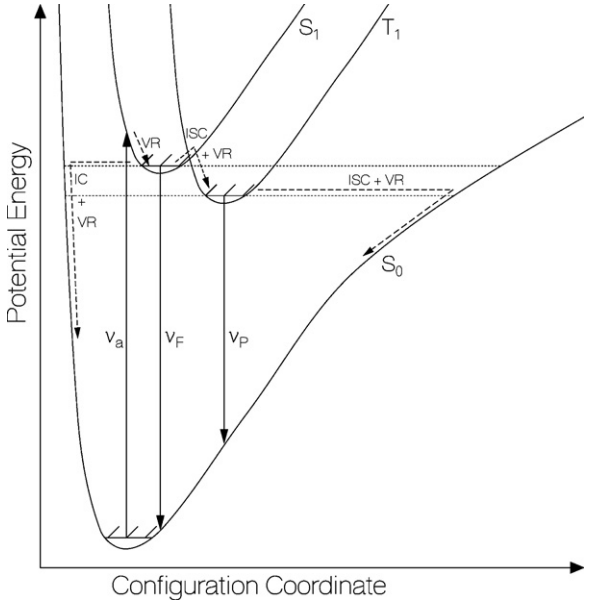

Fig. 6. Potential energy surface scheme. ν_a: excitation frequency; ν_F: fluorescence emission frequency; ν_P: phosphorescence emission frequency; VR: vibronic relaxation; IC: internal conversion; ISC: intersystem-crossing.

of temperature showed in general an increase of the fluorescence efficiency at a high absolute quantum yield level and an increase of phosphorescence efficiency at a low absolute quantum yield level with decreasing temperature. For ER in starch a strong increase in phosphorescence efficiency with decreasing temperature was measured at a reasonably high absolute quantum yield level ($\phi_P(293\,K) \approx 0.06$, $\phi_P(12\,K) \approx 0.25$). For RB the phosphorescence quantum yield was roughly temperature independent at an absolute quantum yield level of 1–3%.

The obtained quantum yields of photoluminescence ϕ_L, fluorescence ϕ_F, and phosphorescence ϕ_P are collected in Table 1. Additionally values of the quantum yields of S_1–S_0 internal conversion ϕ_{IC,S_1-S_0}, S_1–T_1 intersystem-crossing ϕ_{ISC,S_1-T_1}, non-radiative S_1-state depopulation, $\phi_{S_1,nr} = 1 - \phi_F = \phi_{IC,S_1-S_0} + \phi_{ISC,S_1-T_1}$, true triplet-state based phosphorescence [2], $\phi'_P = \phi_P/\phi_{ISC,S_1-T_1}$, and T_1-S_0 intersystem-crossing, $\phi_{ISC,T_1-S_0} = 1 - \phi'_P$ are included in Table 1. At room temperature ϕ_{IC,S_1-S_0} and ϕ_{ISC,S_1-T_1} were determined in [2]. At 12 K we can only give intervals for ϕ_{IC,S_1-S_0} and ϕ_{ISC,S_1-T_1} by the relations:

$$\phi_{S_1,nr}(12\,K) - \phi_{ISC,S_1-T_1}(293\,K) < \phi_{IC,S_1-S_0}(12\,K) < \min[\phi_{IC,S_1-S_0}(293\ K), \phi_{S_1,nr}(12\,K) - \phi_P(12\,K)] \quad (3)$$

and

$$\max[\phi_{S_1,nr}(12\ K) - \phi_{IC,S_1-S_0}(293\,K), \phi_P(12\,K)] < \phi_{ISC,S_1-T_1}(12\,K) < \min[\phi_{ISC,S_1-T_1}(293\ K), \phi_{S_1,nr}(12\,K)] \quad (4)$$

assuming that ϕ_{IC,S_1-S_0} and ϕ_{ISC,S_1-T_1} decrease with decreasing temperature (see below).

For a discussion of the luminescence behavior schematic potential energy curves of the S_0 singlet ground-state, the first exited singlet state S_1, and the first triplet state T_1 are shown in Fig. 6. The non-crossing and non-touching S_0 and S_1 potential energy curves are called spectroscopic states according to [35]. The excitation light (frequency ν_a) excites molecules from the S_0-ground-state to a Franck–Condon position in the S_1-state with some excess energy. From the Franck–Condon excited position the molecule relaxes to a thermal equilibrium position (potential energy minimum) in the S_1 state by vibronic relaxation (VR). The excess energy is transferred to the host matrix. From the thermal equilibrium position, there occurs S_1–S_0 fluorescence emission (spontaneous emission of photons of frequency ν_F), equi-potential S_1–S_0 internal conversion (IC) with subsequent S_0-state vibronic relaxation (VR), and thermal activated S_1–T_1 intersystem-crossing (ISC) with subsequent vibronic relaxation (VR). Spin–orbit coupling causes avoided crossing of the S_1–T_1 potential energy curves [35] and it lowers the activation barrier (not shown in figure). The molecules transferred to the T_1 state thermalize there and relax to the S_0 ground-state by phosphorescence emission (spontaneous emission of photons of frequency ν_P) and equi-potential T_1–S_0 intersystem-crossing (ISC) with subsequent vibronic relaxation (VR). Thermally populated vibronic states in the S_0, S_1, and T_1 potential energy curve valleys are indicated by hatched regions in Fig. 6. Fluorescence and phosphorescence quenching by impurities (like molecular oxygen) is neglected since in solid matrices diffusional approach of dye molecules and impurity centers does not occur.

The presented schematic of Fig. 6 indicates the following dynamics features: (i) the rate of S_1–S_0 spontaneous emission, $k_{rad,S_1-S_0} = \tau^{-1}_{rad,S_1-S_0}$, is temperature independent, (ii) the equi-potential S_1–S_0 internal conversion rate, k_{IC,S_1-S_0}, is in zero-order approximation temperature independent and in first-order approximation decreases with decreasing temperature (higher internal conversion rate from thermally excited vibronic states than from electronic ground-state due to vibronic coupling, reduction of vibronic excited states at low temperatures, lowering of ϕ_{IC,S_1-S_0} with decreasing temperature), (iii) the thermal activated S_1–T_1 intersystem-crossing rate, k_{ISC,S_1-T_1}, decreases with decreasing temperature (lowering of ϕ_{ISC,S_1-T_1} with decreasing temperature), but spin–orbit coupling leads to avoided crossing of the S_1 and T_1 potential energy curves and lowers the activation barrier [35], (iv) the rate of T_1–S_0 spontaneous emission, $k_{rad,T_1-S_0} = \tau^{-1}_{rad,T_1-S_0}$, is temperature independent, and (v) the equi-potential T_1–S_0 intersystem-crossing rate, k_{ISC,T_1-S_0}, is in zero-order approximation temperature independent and in first-order approximation decreases with decreasing temperature (higher intersystem-crossing rate from thermally excited vibronic states than from electronic ground-state due to vibronic coupling, reduction of vibronic excited states at low temperatures, lowering of ϕ_{ISC,T_1-S_0} with decreasing temperature).

In the case of FL in the biopolymers the fluorescence quantum yield at room temperature was already rather high and it increased by 2–19% at 12 K. The efficiency of S_1-state non-radiative decay, $\phi_{S_1,nr} = 1 - \phi_F$, decreased with decreasing temperature (see Table 1) indicating reduction of S_1–S_0 internal conversion at low temperatures. A quantum yield of S_1–T_1 intersystem-crossing of approximately 3% was reported at 77 K [36] and at room temperature [37–39]. A low efficiency of intersystem crossing is expected by low spin–orbit coupling in the absence of heavy atoms. Phosphorescence could not be well resolved because of its low efficiency.

In the case of DBF in the biopolymers the quantum yield of phosphorescence was quite low at room temperature ($\phi_P \approx 0.003$ [2]) and it increased with deceasing temperature but remained below 2% even at 12 K (see Table 1) The efficiency of S_1–T_1 intersystem crossing at room temperature was 15–25% [2] due to the Br heavy-atom effect. It is thought to decrease with decreasing temperature due to aggravation of S_1–T_1 barrier crossing. The T_1–S_0 intersystem-crossing efficiency decreased with decreasing temperature favoring phosphorescence emission. Despite lower T_1 state population due to the lower S_1–T_1 intersystem crossing rate the phosphorescence efficiency increased with decreasing temperature at a low absolute level because of decreasing T_1–S_0 intersystem-crossing.

The fluorescence efficiency of EO in the biopolymers increased with decreasing temperature (decrease of S_1–S_0 internal conver-

sion and decrease of S_1–T_1 intersystem crossing with decreasing temperature). The phosphorescence behavior of EO in the biopolymers is similar to the case of DBF in the biopolymers. The phosphorescence quantum yield at room temperature was found to be $\phi_P \approx 0.006$ [2] and the present measurements give $\phi_P = 0.0073$ (gelatin) to $\phi_P = 0.018$ (chitosan) at 12 K. The efficiency of S_1–T_1 intersystem crossing at room temperature is around 20% [2] and it is reduced at low temperature. The phosphorescence efficiency increased at low temperature despite reduced triplet state population because of overcompensation by the reduced T_1–S_0 intersystem crossing at low temperatures.

In the case of ER the fluorescence efficiency increased with decreasing temperature due to less S_1–S_0 internal conversion at low temperature. The S_1–T_1 intersystem crossing efficiency was in the 37–56% range at room temperature and remained in the 30–40% range at 12 K due to the heavy-atom induced spin–orbit coupling (with nearly barrier-less transition from S_1 to T_1). The quantum yield of phosphorescence increased with decreasing temperature due to lowering of T_1–S_0 intersystem crossing efficiency at low temperature.

RB behaved similar to ER in the temperature dependence of fluorescence and phosphorescence. The efficiency of S_1–T_1 intersystem-crossing is higher in RB than in ER (in 60–80% range both at room temperature and low temperature, stronger heavy-atom induced spin–orbit coupling) but the phosphorescence efficiency is lower in RB than in ER both at room temperature and low temperature because of more efficient T_1–S_0 intersystem-crossing of RB compared to ER.

5. Conclusions

The temperature dependence of the photoluminescence of disodium fluorescein (FL), 4,5-dibromine fluorescein (DBF), disodium tetrabromine fluorescein (EO), disodium tetraiodine fluorescein (ER), and disodium tetrachlorine–tetraiodine fluorescein in a protein film (gelatin), a polysaccharide film (starch), and a polyaminosaccharide film (chitosan) was studied. In a general trend the fluorescence increased with decreasing temperature at a high level of absolute quantum yield due to lower S_1–S_0 internal conversion and lower S_1–T_1 intersystem crossing at low temperature. The phosphorescence efficiency in a general trend increased with decreasing temperature at a low absolute quantum yield level due to an interplay of reduction of thermal activated S_1–T_1 intersystem crossing (less triplet population) and a reduction of T_1–S_0 intersystem crossing (larger true T_1-state based phosphorescence ϕ'_P) at low temperatures.

The temperature dependent luminescence studies on the selected fluorone dyes were carried out in biopolymer hosts. A similar temperature dependent luminescence behavior of the investigated fluorone dyes is expected in other solid-state hosts like organic polymers (e.g. PVA [23] or PMMA [31]).

The observed temperature dependence of the photoluminescence of the studied fluorone dyes in some solid-state biopolymer hosts is thought to apply rather generally to dyes of spectroscopic-state potential energy surfaces (like laser dyes) in transparent solid hosts where fluorescence and phosphorescence quenching by impurities (like molecular oxygen) may be negligible. The situation is different for dyes in liquid solvents at room temperature which freeze at low temperature. In this situation the room temperature phosphorescence is quenched by dye and impurity center diffusion causing diffusion controlled dye-impurity quenching and dye-dye self-annihilation [32,33].

Acknowledgements

A.P. is grateful to Prof. F.J. Gießibl for his kind hospitality. T.T. thanks the Japan Society for Promotion of Science for financial support (the Grant-in-Aid for the Scientific Research, Project No C-22560013) and Mr. Y. Nakai for help in the photoluminescence measurements at low temperatures.

References

[1] E. Slyusareva, A. Sizykh, A. Tyagi, A. Penzkofer, Spectral and photophysical properties of fluorone dyes in biorelated films and methanol, J. Photochem. Photobiol. A: Chem. 208 (2009) 131–140.
[2] A. Tyagi, A. Penzkofer, E. Slyusareva, A. Sizykh, Phosphorescence and delayed fluorescence properties of fluorone dyes in bio-related films, Chem. Phys. 378 (2010) 58–65.
[3] R.A.A. Muzzarelli (Ed.), Chitosan Per Os: From Dietary Supplement to Drug Carrier, Atec, Grottammare, 2000.
[4] K.G. Skryabin, G.A. Vihoreva, V.P. Varlamova (Eds.), Chitin and Chitosan: Production, Properties and Application, Nauka, Moskva, 2002.
[5] P.J. VandeVord, H.W.T. Matthew, S.P. DeSilva, L. Mayton, B. Wu, P.H. Wooley, Evaluation of the biocompatibility of a chitosan scaffold in mice, J. Biomed. Mater. Res. 59 (2002) 505–590.
[6] X. Qu, A. Wirsén, A.-C. Albertsson, Novel pH-sensitive chitosan hydrogels: swelling behavior and states of water, Polymer 41 (2000) 4589–4598.
[7] E.I. Kulish, R.R. Fatkullina, V.P. Volodina, S.V. Kolesov, Yu.B. Monakov, Enzymatic degradation of modified chitosan films, Russ. J. Appl. Chem. 80 (2007) 1178–1180.
[8] V. Kratasyuk, E. Esimbekova, Polymer immobilized bioluminescent systems for biosensors and bioinvestigations, in: R. Arshady (Ed.), Polymeric Biomaterials, The PBM Series vol. 1, Citus Books, London, 2003, pp. 301–343.
[9] D. Magde, R. Wong, P.L. Seybold, Fluorescence quantum yields and their relation to lifetimes of rhodamine 6G and fluorescein in nine solvents: improved absolute standards for quantum yields, Photochem. Photobiol. 75 (2002) 327–334.
[10] R. Sjöback, J. Nygren, M. Kubista, Absorption and fluorescence properties of fluorescein, Spectrochim. Acta A 51 (1995) L1–L21.
[11] M.M. Martin, Hydrogen bond effects on radiationless electronic transitions in xanthene dyes, Chem. Phys. Lett. 35 (1975) 105–111.
[12] N.B. Joshi, P. Gangola, D.D. Pant, Internal heavy atom effect on the radiative and non-radiative rate constants in xanthene dyes, J. Lumin. 21 (1979) 111–118.
[13] L.S. Forster, D. Dudley, The luminescence of fluorescein dyes, J. Phys. Chem. 66 (1962) 838–840.
[14] K. Gollnick, T. Franken, M.F.R. Fouda, H.R. Paur, S. Held, Merbromin (mercurochrome) and other xanthene dyes: quantum yields of triplet sensitzer generation and singlet oxygen formation in alcoholic solutions, J. Photochem. Photobiol. B: Biol. 12 (1992) 57–81.
[15] P.G. Seybold, M. Gouterman, J. Callis, Calorimetric, photometric and lifetime determinations of fluorescence yields of fluorescein dyes, Photochem. Photobiol. 9 (1969) 229–242.
[16] V. Zanker, W. Körber, Fluoreszenz- und Phosphoreszenzausbeute sowie Lebensdauer Messungen an dihalogenierten Acridinen und Fluoreszeinen Z, Angew. Phys. 14 (1962) 43–48.
[17] C.A. Parker, C.G. Hatchard, Triplet-singlet emission in fluid solutions. Phosphorescence of eosin, Trans. Faraday Soc. 57 (1961) 1894–1904.
[18] G.R. Fleming, A.W.E. Knight, J.M. Morris, R.J.S. Morrison, G.W. Robinson, Picosecond fluorescence studies of xanthene dyes, J. Am. Chem. Soc. 99 (1977) 4306–4311.
[19] P.V. Kamat, M.A. Fox, Photophysics and photochemistry of xanthene dyes in polymer solutions and films, J. Phys. Chem. 88 (1984) 2297–2302.
[20] D.S. McClure, Triplet–singlet transitions in organic molecules. Lifetime measurements of the triplet state, J. Chem. Phys. 17 (1949) 905–913.
[21] S.P. McGlynn, T. Azumi, M. Kinoshita, Molecular Spectroscopy of Triplet State, Prentice Hall, Englewood Cliffs, NJ, 1969.
[22] N.J. Turro, Molecular Photochemistry, W.A. Benjamin, Inc., New York, 1978.
[23] P.M. Lettinga, H. Zuilhof, M.A.M.J. van Zandvoort, Phosphorescence and fluorescence characterization of fluorescein derivatives immobilized in various polymer matrices, Phys. Chem. Chem. Phys. 2 (2000) 3697–3707.
[24] M. Zander, G. Kirsch, On the phosphorescence of benzologues of furan, thiophene, selenophene, and tellurphene, Z. Naturfoschung 44a (1989) 205–209.
[25] T. Tsuboi, A.K. Bansal, A. Penzkofer, Temperarature dependence of fluoresecence and phosphorescence of the triphenylamine dimer 3-methyl-TPD, Opt. Mater. 31 (2005) 980–988.
[26] C. Moore, D. Boxer, P. Garland, Phosphorescence depolarization and the measurement of rotational motion of proteins in membranes, FEBS Lett. 108 (1979) 161–166.
[27] P. Johnson, P.B. Garland, Fluorescent triplet probes for measuring the rotational diffusion of membrane proteins, Biochem. J. 203 (1982) 313–321.
[28] N. Velasco-García, R. Pereiro-García, M. Diaz-García, Analytical and mechanistic aspects of the room temperature phosphorescence of erythrosine B adsorbed on solid supports as oxygen sensing phases, Spectrochim. Acta A 51 (1995) 895–904.
[29] S.K. Lam, E. Namdas, D. Lo, Effects of oxygen and temperature on phosphorescence and delayed fluoresecence of erythrosine B trapped in sol–gel silica, J. Photochem. Photobiol. A: Chem. 118 (1998) 25–30.
[30] L.C. Pravinata, Y. You, R.D. Ludescher, Erythrosine B phosophorescence monitors molecular mobility and dynamic site heterogeneity in amorphous sucrose, Biophys. J. 88 (2005) 3551–3561.

[31] R. Duchowicz, M.L. Ferrer, A.U. Acuña, Kinetic spectroscopy of erythrosine phosphorescence and delayed fluorescence in aqueous solution at room temperature, Photochem. Photobiol. 68 (1998) 494–501.
[32] C.A. Parker, Photoluminescence of Solutions, Elsevier, Amsterdam, 1968.
[33] J.B. Birks, Photophysics of Aromatic Molecules, Wiley-Interscience, London, 1970.
[34] R.W. Chambers, D.R. Kearns, Triplet states of some common photosensitizing dyes, Photochem. Photobiol. 10 (1969) 215–219.
[35] N.J. Turro, V. Ramamurthy, J.C. Scaiano, Principles of Molecular Photochemistry. An Introduction, University Science Books, Sausalito, CA, 2009.
[36] Z.-C. Bi, Q.-S. Xie, J.-Y. Yu, Photochemical hydrogen evolution from alkaline solutions of xanthene dyes, J. Photochem. Photobiol. A 85 (1995) 269–273.
[37] B. Soep, A. Kellmann, M. Martin, L. Lindqvist, Study of triplet quantum yields using a tunable dye laser, Chem. Phys. Lett. 13 (1972) 241–244.
[38] E. Gandin, Y. Lion, A. van de Vorst, Quantum yield of singlet oxygen production by xanthene derivatives, Photochem. Photobiol. 37 (1983) 271–278.
[39] P.G. Bowers, G. Porter, Triplet state quantum yields for some aromatic hydrocarbons and xanthene dyes in dilute solution, Proc. R. Soc. A 299 (1967) 348–352.